Eidgenössische Technische Hochschule Zürich
Swiss Federal Institute of Technology Zurich

Seminar for Applied Mathematics SAM

Shape optimization by pursuing diffeomorphisms

R. Hiptmair and A. Paganini

Research Report No. 2014-27

October 2014
Latest revision: December 2014

Seminar für Angewandte Mathematik
Eidgenössische Technische Hochschule
CH-8092 Zürich
Switzerland

Funding: This research was supported by ETH Zurich through the CHIRP project CH1-02 11-1

Shape optimization by pursuing diffeomorphisms

R. Hiptmair and A. Paganini

December 17, 2014

Abstract

We consider PDE constrained shape optimization in the framework of finite element discretization of the underlying boundary value problem. We present an algorithm tailored to preserve and exploit the approximation properties of the finite element method, and that allows for arbitrarily high resolution of shapes. It employs (i) B-spline based representations of the deformation diffeomorphism, and (ii) superconvergent domain integral expressions for the shape gradient. We provide numerical evidence of the performance of this method both on prototypical well-posed and ill-posed shape optimization problems.

1 Introduction

Physical phenomena are described by mathematical models that link input and output quantities. An important task in engineering is to find optimal values of the input so that a target output is minimized. In shape optimization the target output depends on the shape Ω of an object. This dependence is modeled via a shape functional $\mathcal{J}$.

In several relevant applications the shape functional $\mathcal{J}$ depends, additionally, on the solution of a boundary value problem (BVP) stated on Ω. In this case we speak of PDE constrained shape optimization. These optimization problems are highly non-linear and can rarely be solved analytically. Usually, one has to content oneself with approximate optimal shapes obtained with iterative optimization algorithms combined with approximate solutions of the underlying BVP. Clearly, the quality of the approximate optimal shapes heavily depends on the choice of the numerical method used to retrieve them.

An accurate method to solve PDE constrained optimization problems has been developed relying on boundary element method solutions of the underlying BVP [16, 17]. However, the bulk of literature considers discretizations

by means of the finite element method (FEM) [2, 6–8, 18, 23–26, 28]. In this case we can distinguish between moving-mesh and fixed-mesh methods.

The former discretize an initial guess Ω_0 with a mesh and then optimize the coordinates of the mesh nodes [2, 26, 28]. This is a very delicate task because the mesh might get distorted or self-intersect as the optimization routine proceeds [3, 4].

Among the fixed-mesh methods, the two most popular approaches are level-set methods and free-form deformation methods. In the level-set approach, the boundary of the optimal domain is represented as the zero-level of a function [5]. The optimization is then carried out by updating this function. Again, this is a delicate process because, to identify the boundary of the optimized domain, the level set function should have steep slope at the zero-level. However, as the optimization proceeds, it is observed that level-functions tend to become flat [27].

On the other hand, free-form deformation methods [7, 24] recast the shape optimization problem as an optimal control problem. Shapes are parametrized by applying a transformation to the initial guess Ω_0. This transformation is constructed with (piecewise) polynomials defined on a lattice of control points, and optimization is carried out on their coordinates. This approach allows to preserve the approximation properties of FEM. However, the infinite dimensional shape optimization problem is replaced with a counterpart with a fixed small number of control parameters, and the dependence of the quality of the discrete solution on the number of control parameters is not clear.

We present an algorithm developed to preserve and exploit the approximation properties of FEM, and that allows for arbitrarily high resolution of shapes. Similar to the free-form deformation approach, we recast the shape optimization problem as an optimal control problem. Shapes are parametrized by letting a diffeomorphism act on an initial shape Ω_0. Pursuing a Ritz approach, we discretize the diffeomorphism with conforming basis functions based on cubic B-splines. We show that, under reasonable assumptions, the sequence of optimal discrete solutions converges to the global minimum as the dimension of the trial space tends to infinity. We also investigate the impact of FEM approximations in the context of elliptic PDE constrained shape optimization and formulate a descent method that enjoys superconvergence in the approximation of the Fréchet derivative. We test the performance of the proposed method both on a well-posed model problem stemming from the class of exterior Bernoulli free boundary problems and on a prototypical ill-posed inverse problem.

2 Shape optimization in parametric form

Let $D \subset \mathbb{R}^d$ be bounded and convex domain (hold-all domain), and let Ω_0 be a compact subset of D with Lipschitz boundary. We fix $\varepsilon > 0$ and define the set of admissible shapes as

$$\mathcal{U}_{\mathrm{ad}}(\Omega_0) \coloneqq \{T_{\mathcal{V}}(\Omega_0);\, T_{\mathcal{V}} = \mathcal{I} + \mathcal{V}, \|\mathcal{V}\|_{C^1(\overline{D};\mathbb{R}^d)} \leq 1 - \varepsilon\}\,. \tag{1}$$

Note that the map $T_{\mathcal{V}} \coloneqq \mathcal{I}+\mathcal{V}$ is a diffeomorphism whenever $\|\mathcal{V}\|_{C^1(\overline{D};\mathbb{R}^d)} < 1$ [2, Lemma 6.13]. Let $\mathcal{J}$ be a real-valued functional defined on $\mathcal{U}_{\mathrm{ad}}(\Omega_0)$, and let $\tilde{\mathcal{J}}$ be defined by

$$\tilde{\mathcal{J}} : B^1_{1-\varepsilon} \to \mathbb{R}\,; \quad \mathcal{V} \mapsto \mathcal{J}\left(T_V(\Omega_0)\right)\,.$$

where $B^k_{1-\varepsilon}$ denotes the closed ball in $C^k(\overline{D};\mathbb{R}^d)$ of radius $1-\varepsilon$ centered in 0. The shape optimization problem

$$\inf_{\Omega \in \mathcal{U}_{\mathrm{ad}}(\Omega_0)} \mathcal{J}(\Omega)$$

can be recast as

$$\inf_{\mathcal{V} \in B^1_{1-\varepsilon}} \tilde{\mathcal{J}}(\mathcal{V})\,. \tag{2}$$

Theorem 1. *Let $\tilde{\mathcal{J}}$ be continuous with respect to the $C^1(\overline{D};\mathbb{R}^d)$- norm and restrict the shape optimization problem* (2) *to*

$$\inf_{\mathcal{V} \in B^2_{1-\varepsilon}} \tilde{\mathcal{J}}(\mathcal{V})\,. \tag{3}$$

Then, there exist a vector field $\mathcal{V}^* \in C^1(\overline{D};\mathbb{R}^d)$ so that

$$\tilde{\mathcal{J}}(\mathcal{V}^*) = \inf_{\mathcal{V} \in B^2_{1-\varepsilon}} \tilde{\mathcal{J}}(\mathcal{V})\,.$$

Proof. We follow closely [2, Thm 5.12]. The main ingredient is the compact embedding $C^2(\overline{D};\mathbb{R}^d) \overset{c}{\hookrightarrow} C^1(\overline{D};\mathbb{R}^d)$, which holds for D convex or, more generally, if "every pair of points $x, y \in D$ can be joined with a rectifiable arc in D having length not exceeding some fixed multiple of $|x-y|$" [1, Thm 1.34].

A minimizing sequence of (3) is bounded (by definition of the optimization problem). Thus, by compactness, we can extract a subsequence that converges to a limit function $\hat{\mathcal{V}}$ in the $C^1(\overline{D};\mathbb{R}^d)$-norm. Finally, the continuity assumption on $\tilde{\mathcal{J}}$ implies $\hat{\mathcal{V}} = \mathcal{V}^*$. □

Remark 1. *The continuity assumption on $\tilde{\mathcal{J}}$ in Theorem 1 is fulfilled by most of the shape functionals considered in literature. For instance, this is the case for the volume and the surface area shape functionals.*

Remark 2. *A counterpart of Theorem 1 still holds if the function spaces $C^1(\overline{D};\mathbb{R}^d), C^2(\overline{D};\mathbb{R}^d)$ are replaced by $W^{1,\infty}(\mathbb{R}^d;\mathbb{R}^d), W^{2,\infty}(\mathbb{R}^d;\mathbb{R}^d)$, respectively. However, having approximations by means of the Ritz method in mind, we restrict our framework to separable spaces.*

Remark 3. *There is little hope for uniqueness in this framework. Let $\mathcal{V}^*$ be an optimal solution. If there is a vector field $\tilde{\mathcal{V}} \neq \mathcal{I}$ so that $\tilde{\mathcal{V}}(\partial\Omega_0) = \partial\Omega_0$ (from the set point of view), then the composition $\mathcal{V}^* \circ (\mathcal{I} + \tilde{\mathcal{V}})$ is an optimal solution, too.*

Approximate solutions can be obtained easily with a Ritz approach.

Theorem 2. *Let $\{V_N\}_{N\in\mathbb{N}}$ be a nested sequence of $C^2(\overline{D};\mathbb{R}^d)$-conforming trial spaces that satisfies*

$$\overline{\cup_{N\in\mathbb{N}} V_N}^{C^2(\overline{D};\mathbb{R}^d)} = C^2(\overline{D};\mathbb{R}^d)\,.$$

Let $\{\mathcal{V}_N^*\}_{N\in\mathbb{N}}$ be the sequence of discrete solutions defined by

$$\mathcal{V}_N^* \in \operatorname*{argmin}_{\mathcal{V}_N \in V_N \cap B^2_{1-\varepsilon}} \tilde{\mathcal{J}}(\mathcal{V}_N)\,. \tag{4}$$

Then, under the assumptions of Theorem 1, $\{\mathcal{V}_N^*\}_{N\in\mathbb{N}}$ is a minimizing sequence of $\tilde{\mathcal{J}}$.

Proof. We follow closely the proof of the classic result on the convergence of Ritz methods given in [19, Sect. 40.1].

Let $\mu \in \mathbb{R}$ be the infimum of (3). Note that $\mu > -\infty$. Let $a > 0$, and let $\mathcal{V} \in B^2_{1-\varepsilon}$ satisfy

$$\tilde{\mathcal{J}}(\mathcal{V}) < \mu + a\,.$$

By continuity of $\tilde{\mathcal{J}}$, $\mathcal{V}$ can be rescaled so that

$$\|\mathcal{V}\|_{C^2(\overline{D};\mathbb{R}^d)} < 1 - \varepsilon \quad \text{and} \quad \tilde{\mathcal{J}}(\mathcal{V}) < \mu + 2a\,.$$

Let $b > 0$, and let $N = N(b) \in \mathbb{N}$ be sufficiently large. Then, there exists a $\mathcal{V}_N \in V_N \cap B^2_{1-\varepsilon}$ that satisfies

$$\|\mathcal{V} - \mathcal{V}_N\|_{C^2(\overline{D};\mathbb{R}^d)} < b\,.$$

Furthermore, for $b = b(a)$ small enough, it holds

$$\tilde{\mathcal{J}}(\mathcal{V}_N) < \mu + 3a\,.$$

Let $\mathcal{V}_N^*$ be defined as in (4). It holds

$$\mu \leq \tilde{\mathcal{J}}(\mathcal{V}_N^*) \leq \tilde{\mathcal{J}}(\mathcal{V}_N) \leq \mu + 3a\,.$$

Since a is arbitrary, it follows

$$\lim_{N\to\infty} \tilde{\mathcal{J}}(\mathcal{V}_N^*) = \mu\,.$$

□

Remark 4. *More sophisticated convergence theories can be found in [17, 18, 23]. These articles rely on a parametrization of the boundary, and consider as admissible shapes those that can be reached via a normal perturbation of the boundary $\partial\Omega_0$. In this case, uniqueness of the optimal solution can be achieved, and a priori convergence rates can be proved.*

3 PDE constrained shape optimization

In PDE constrained shape optimization, the goal is to find the domain Ω that minimizes the functional $\mathcal{J}(\Omega, u)$ subject to a PDE constraint $\mathcal{A}u = f$ in Ω. Here, $\mathcal{A} : X(\Omega) \to X(\Omega)^*$ denotes a second order $X(\Omega)$-elliptic operator between the Hilbert space $X(\Omega)$ and its dual $X(\Omega)^*$, which are function spaces on the domain Ω. Similarly as in (2), the shape optimization problem can be recast in a parametric form relying on the characterization of admissible domains (1), that is,

$$\inf_{\mathcal{V}\in B^1_{1-\varepsilon}} \tilde{\mathcal{J}}(\mathcal{V}, u), \quad \text{subject to} \quad \tilde{\mathcal{A}}_{\mathcal{V}} u = \tilde{f}_{\mathcal{V}} \text{ in } \Omega_0\,. \tag{5}$$

Both the elliptic operator $\tilde{\mathcal{A}}_{\mathcal{V}} : X(\Omega_0) \to X(\Omega_0)^*$ and the linear functional $\tilde{f}_{\mathcal{V}} \in X(\Omega_0)^*$ depend on the vector field $\mathcal{V}$ and are created in a way so that $u \in X(\Omega_0)$ is the solution to $\tilde{\mathcal{A}}_{\mathcal{V}} u = \tilde{f}_{\mathcal{V}}$ in Ω_0 if and only if $\hat{u} := u \circ T_{\mathcal{V}}^{-1} \in X(\Omega)$ is the solution to $\mathcal{A}\hat{u} = f$ in Ω.

The idea of recasting both the shape functional and the PDE constraint on a reference domain is not new to shape optimization. It has already been used, for instance, in [8,18,25,26], and is, de facto, the standard approach for shape optimization based on free-form deformations; see [7,24] and references therein.

Example 1. *The parametric form of the shape optimization problem*

$$\inf_{\mathcal{V}\in\mathcal{U}_{\mathrm{ad}}(\Omega_0)} \mathcal{J}(\Omega,u), \quad \textit{subject to} \quad -\Delta u = f \ \textit{in}\ H_0^1(\Omega)\,, \tag{6}$$

with $\mathcal{J}(\Omega,u) \coloneqq \int_\Omega j(u)\mathrm{d}\boldsymbol{x}$, $j\in C^1(\mathbb{R})$ *and* $f\in H^{-1}(\Omega)$, *reads*

$$\begin{aligned} &\inf_{\mathcal{V}\in B^1_{1-\varepsilon}} \tilde{\mathcal{J}}(\mathcal{V},u)\,, \quad \textit{subject to} \\ &-\operatorname{div}(\mathbf{M}_{\mathcal{V}}\,\mathbf{grad}\,u) = (\det \mathbf{D}T_{\mathcal{V}})T_{\mathcal{V}}^*(f) \ \textit{in}\ H_0^1(\Omega_0)\,, \end{aligned} \tag{7}$$

where the pullback $T_{\mathcal{V}}^*$ *is defined as the composition* $T_{\mathcal{V}}^*(f) \coloneqq f\circ T_{\mathcal{V}}$,

$$\tilde{\mathcal{J}}(\mathcal{V},u) \coloneqq \int_{\Omega_0} j(u)(\det \mathbf{D}T_{\mathcal{V}})\mathrm{d}\boldsymbol{x}\,, \quad \textit{and} \quad \mathbf{M}_{\mathcal{V}} \coloneqq (\det \mathbf{D}T_{\mathcal{V}})\mathbf{D}T_{\mathcal{V}}^{-1}\mathbf{D}T_{\mathcal{V}}^{-T}\,.$$

Assuming continuity of the map $\mathcal{V}\mapsto\tilde{\mathcal{J}}(\mathcal{V},u)$ on $C^1(\overline{D};\mathbb{R}^d)$, an approximate solution of (5) can be obtained as in Theorem 2 by computing

$$\mathcal{V}_N^* \in \operatorname*{argmin}_{\mathcal{V}_N\in V_N\cap B^2_{1-\varepsilon}} \tilde{\mathcal{J}}(\mathcal{V}_N,u), \quad \text{subject to} \quad \tilde{\mathcal{A}}_{\mathcal{V}_N}u = \tilde{f}_{\mathcal{V}_N} \text{ in } \Omega_0 \tag{8}$$

for N large enough. The approximate optimal solution $\mathcal{V}_N^*$ must satisfy the variational inequality [20, Thm 1.48]

$$d\tilde{\mathcal{J}}(\mathcal{V}_N^*,u;\mathcal{W}_n-\mathcal{V}_N^*)\geq 0 \quad \text{for all} \quad \mathcal{W}_N\in V_N\cap B^2_{1-\varepsilon}\,, \tag{9}$$

where $d\tilde{\mathcal{J}}$ denotes the Fréchet derivative of $\tilde{\mathcal{J}}$. It can be retrieved with descent methods, which converge in $C^1(\overline{D};\mathbb{R}^d)$ due to the compactness of $V_N\cap B^2_{1-\varepsilon}$. More details on the algorithm are given in Section 4.

Remark 5. *In example 1, a minimizing sequence* $\{\mathcal{V}_N^*\}_{N\in\mathbb{N}}$ *of* (8) *has a subsequence* $\{\mathcal{V}_{N_i}^*\}_{i\in\mathbb{N}}$ *that converges strongly in the* $C^1(\overline{D};\mathbb{R}^d)$*-norm to a* $\hat{\mathcal{V}}\in C^1(\overline{D};\mathbb{R}^d)$. *Therefore, the ellipticity constants of* $\{\tilde{\mathcal{A}}_{\mathcal{V}_{N_i}}\}_{i\in\mathbb{N}}$ *are bounded from below by a constant* $c>0$. *This implies that*

$$\|u_{\tilde{\mathcal{V}}}-u_{N_i}\|_{H^1(\Omega_0)}\to 0 \quad \textit{as}\ i\to\infty\,,$$

where u_{N_i} *is the solution to* $\tilde{A}_{\mathcal{V}_{N_i}}u=\tilde{f}_{\mathcal{V}_{N_i}}$ *and* $u_{\tilde{\mathcal{V}}}$ *is the solution to* $\tilde{A}_{\hat{\mathcal{V}}}u=\tilde{f}_{\hat{\mathcal{V}}}$, *see [2, Lemma 5.3]. With this result it is easy to show* $C^1(\overline{D};\mathbb{R}^d)$*-continuity of the constraint functional* (7).

4 Algorithm and implementation

We focus on the optimization problem (8). Let $\Omega_0 \subset D$ be an initial guess. As trial space V_N, we choose the space spanned by multivariate B-splines of degree 3 generated on a regular grid that covers the hold-all domain D; see [22, Sect. 7.3]. Note that the hold-all domain D can be chosen to have a simple shape, e.g., a product domain. More precisely, vector fields belonging to V_n can be written as

$$\mathcal{V}_N = \sum_{i=1}^{N} \mathbf{B}_i \sum_{j=1}^{d} c_i^j \mathbf{e}_j \,, \quad c_i^j \in \mathbb{R} \,, \tag{10}$$

where $\mathbf{B}_i$ denotes the i-th multivariate B-spline of degree 3, and $\mathbf{e}_j$, $j = 1, \ldots, d$, are basis vectors of $\mathbb{R}^d$.

The trial space V_N fulfills the assumptions of Theorem 2: it contains tensorized polynomials by Marsden's Identity [22, Sect 4.3], and it is $C^2(\overline{D}; \mathbb{R}^d)$-conforming because multivariate B-splines of degree 3 are twice continuously differentiable by construction. Moreover, B-splines have compact support and are polynomial in each grid cell. These two properties are crucial for an efficient implementation of the algorithm. Finally, using B-splines defined on a regular grid greatly simplifies the implementation, because the B-splines $\mathbf{B}_i$ are obtained by translating a single "mother" function [22, Sect. 7.3].

As mentioned in Section 3, an approximation of the discrete optimal solution $\mathcal{V}_N^*$ can be retrieved with descent methods, which rely on the Fréchet derivative $d\tilde{\mathcal{J}}$ of $\tilde{\mathcal{J}}$. Formulas for the Fréchet derivative of $\tilde{\mathcal{J}}$ can easily be derived with the Lagrangian approach described in [20, Sect. 1.6.4]. Note that this approach is simpler than the Lagrangian approach for deriving the Eulerian derivative of $\mathcal{J}(\Omega, u)$ described in [14]; indeed, in the parametric approach described in Section 3, the function space to which u belongs is independent of the control parameter $\mathcal{V}$.

Remark 6. *The Fréchet derivative of $\tilde{\mathcal{J}}(\cdot, u)$ at $\mathcal{V}$ evaluated in the direction $\mathcal{W}$ is equal to the Eulerian derivative of $\mathcal{J}(T_{\mathcal{V}}(\Omega), u)$ in the direction $\mathcal{W} \circ (T_{\mathcal{V}}^{-1})$, because $T_{\mathcal{V}+\mathcal{W}} = T_{\mathcal{W} \circ T_{\mathcal{V}}^{-1}} \circ T_{\mathcal{V}}$.*

Example 2. *The Fréchet derivative of $\tilde{\mathcal{J}}$ from* (7) *reads*

$$d\tilde{\mathcal{J}}(\mathcal{V}, u; \mathcal{W}) = \int_{\Omega_0} (j(u) - fp)\partial_{\mathcal{W}}(\det \mathbf{D}T_{\mathcal{V}}) \\ - \mathbf{grad}\, f \cdot \mathcal{W}p \det \mathbf{D}T_{\mathcal{V}} + \mathbf{grad}\, p \cdot \partial_{\mathcal{W}} \mathbf{M}_{\mathcal{V}} \mathbf{grad}\, u \, \mathrm{d}\boldsymbol{x} \,,$$

where

$$\begin{aligned}\partial_{\mathcal{W}}\mathbf{M}_{\mathcal{V}} &\coloneqq \det(\mathbf{D}T_{\mathcal{V}})\left(\mathrm{tr}(\mathbf{D}T_{\mathcal{V}}^{-1}\mathbf{D}\mathcal{W})\mathbf{D}T_{\mathcal{V}}^{-1}\mathbf{D}T_{\mathcal{V}}^{-T}\right.\\ &\qquad\left.-\mathbf{D}T_{\mathcal{V}}^{-1}(\mathbf{D}T_{\mathcal{V}}^{-T}\mathbf{D}\mathcal{W}^{T}+\mathbf{D}\mathcal{W}\mathbf{D}T_{\mathcal{V}}^{-1})\mathbf{D}T_{\mathcal{V}}^{-T}\right)\,,\\ \partial_{\mathcal{W}}(\det\mathbf{D}T_{\mathcal{V}}) &\coloneqq \det(\mathbf{D}T_{\mathcal{V}})\mathrm{tr}(\mathbf{D}T_{\mathcal{V}}^{-1}\mathbf{D}\mathcal{W})\,,\end{aligned}$$

and where $p \in H_0^1(\Omega_0)$ *is the solution to an adjoint problem*

$$-\operatorname{div}(\mathbf{M}_{\mathcal{V}}\,\mathbf{grad}\,p) = -j'(u)(\det\mathbf{D}T_{\mathcal{V}}) \text{ in } H_0^1(\Omega_0)\,.$$

As Example 2 clearly illustrates, the Fréchet derivative of PDE constrained functionals depends on the solution u of the state problem and, possibly, on the solution p of the adjoint problem. As explicit analytic solution of these boundary value problems are usually not available, one can replace them with approximate solutions, at the cost of introducing a perturbation error when solving the first order optimality condition (9). In particular, this perturbation error both affects the quality of the descent solutions and the stopping criteria in Algorithm 1 on page 11.

We consider here approximations by means of the finite element method. When stated as a volume integral, the map $u \mapsto d\tilde{\mathcal{J}}(\mathcal{V}, u; \mathcal{W})$ is usually continuous with respect to the energy norm of u. Therefore, relying on standard duality techniques, one can expect to observe superconvergence in the approximation of the operator $\tilde{\mathcal{J}}(\mathcal{V}, u; \cdot)$ when the solution u is replaced by its finite element counterpart u_h. The same holds for evaluating the shape functional $\tilde{\mathcal{J}}(\mathcal{V}, u)$. In particular, we consider linear Lagrangian finite elements on quasi-uniform triangular meshes. In this case, it can be shown that

$$|d\tilde{\mathcal{J}}(\mathcal{V}, u; \mathcal{W}) - d\tilde{\mathcal{J}}(\mathcal{V}, u_h; \mathcal{W})| = C(\mathcal{V})h^2\|\mathcal{W}\|_{W^{2,4}(\mathbb{R}^d;\mathbb{R}^d)}\,, \tag{11}$$

where h denotes the width of the finite element mesh and $C(\mathcal{V})$ is a constant that depens on $\mathcal{V}$ and Ω_0. On the other hand, we do not observe superconvergence in (11) when $d\tilde{J}$ is recast as an integration on the boundary $\partial\Omega_0$. We refer to [21] for more details.

The approximate optimal solution $\mathcal{V}_N^*$ is computed iteratively with a descent method as illustrated in Algorithm 1 on page 11. The next paragraphs give a detailed description of the algorithm's steps.

In Line 12 we compute the descent direction. Since the Fréchet derivative $d\tilde{\mathcal{J}}(\mathcal{V}, u; \cdot)$ belongs to the dual space of $C^2(\overline{D}; \mathbb{R}^d)$, its descent direction is usually defined as the solution of [20, Page 103]

$$\inf_{\|\mathcal{W}\|_{C^2(\overline{D};\mathbb{R}^d)}=1} d\tilde{\mathcal{J}}(\mathcal{V}, u; \mathcal{W})\,.$$

However, such a descent direction may not exist because the space $C^2(\overline{D};\mathbb{R}^d)$ is not reflexive.

Employing knowledge on the shape Hessian is also not straightforward, because the second order Fréchet derivative $d^2\tilde{\mathcal{J}}$ cannot be expected to be coercive in the $C^2(\overline{D};\mathbb{R}^d)$-norm. Indeed, for any vector field $\mathcal{W}$ tangential to Ω_0 as well as for vector fields with a compact support that does not intersect $\partial\Omega_0$, it holds[1]

$$d\tilde{\mathcal{J}}(\mathcal{V},u;\mathcal{W}) = 0 \qquad \text{and} \qquad d^2\tilde{\mathcal{J}}(\mathcal{V},u;\mathcal{W},\mathcal{W}) = 0\,.$$

However, in several situations, the shape Hessian is a positive bilinear form when evaluated on vector fields with non-zero normal component on $\partial\Omega_0$. For instance, this is the case for the shape functional defined in (6), see [15]. In the seminal work [13] it has been shown that shape optimization problems admit strict local minima, also called stable minimizers, if the shape Hessian is also coercive with respect to the $H^{1/2}(\partial\Omega_0)$-norm of the normal component of the vector fields, that is,

$$d^2\tilde{\mathcal{J}}(\mathcal{V},u;\mathcal{W},\mathcal{W}) \geq C\|\mathcal{W}\cdot\mathbf{n}\|_{H^{1/2}(\partial\Omega_0)}\,, \tag{12}$$

where $\mathbf{n}$ is the normal vector field on $\partial\Omega_0$ and $C>0$ is a constant independent of $\mathcal{W}$. Thus, coercivity in the $H^{1/2}(\partial\Omega_0)$-norm can be used as a criterion to distinguish between well- and ill-posed shape optimization problems [16]. Therefore, from a theoretical point of view, it is natural to consider the $H^{1/2}(\partial\Omega_0)$-representative of the Fréchet derivative, which is unique up to extensions into the domain D of its values on $\partial\Omega_0$ in the normal direction $\mathbf{n}$. Note that for ill-posed shape optimization problems this choice provides a regularization in the spirit of regularized sequential quadratic programming [11].

We consider here descent directions given as $H_0^1(\overline{D};\mathbb{R}^d)$-representatives of the Fréchet derivative, that is, solutions to the linear system of equations

$$\min_{\|\mathcal{W}\|_{H_0^1(\overline{D};\mathbb{R}^d)}=1} d\tilde{\mathcal{J}}(\mathcal{V},u;\mathcal{W})\,. \tag{13}$$

By the continuity of the normal Dirichlet trace operator

$$H_0^1(\overline{D};\mathbb{R}^d) \to H^{1/2}(\partial\Omega_0)\,, \quad \mathcal{W}\mapsto \mathcal{W}\cdot\mathbf{n}|_{\partial\Omega_0}\,,$$

the $H_0^1(\overline{D};\mathbb{R}^d)$-representative of the Fréchet derivative is the unique $H_0^1(\overline{D};\mathbb{R}^d)$-extension of the normal values of the $H^{1/2}(\partial\Omega_0)$-representative.

[1] The shape gradient $d\tilde{\mathcal{J}}(\mathcal{V},u;\mathcal{W})$ is well-defined for any vector field $\mathcal{W}\in W^{1,\infty}(\mathbb{R}^d;\mathbb{R}^d)$, whilst the shape Hessian requires at least $\mathcal{W}\in W^{2,\infty}(\mathbb{R}^d;\mathbb{R}^d)$ [14].

In Line 15 we check that the transformation $T_{\mathcal{V}}$ is indeed a diffeomorphism. As suggested in [7], we verify that the value of $\det \mathbf{D}T_{\mathcal{V}}$ is bigger than a threshold value[2]. This relaxes the restrictive $C^2(\overline{D};\mathbb{R}^d)$-norm condition in (4) but still guarantees that the algorithm is well-defined. If $\min(\det \mathbf{D}T_{\mathcal{V}})$ is too small we reduce the optimization step until $T_{\mathcal{V}}$ defines a feasible transformation. Note that the while loop terminates due to the continuity of the determinant.

Remark 7. *It might nevertheless happen that the (continuous) optimal solution $\mathcal{V}^*$ lies on the boundary of $B^1_{1-\varepsilon}$, and that, however, the value of $\tilde{\mathcal{J}}(\mathcal{V}^*)$ is not yet satisfactory for convergence purposes. For instance, this might be the case when the initial guess Ω_0 is poorly chosen. In this situation a remedy is to select the retrieved shape as initial guess, and to start the algorithm again. Practically, this can be done by either creating a new mesh of $T_{\mathcal{V}^*}(\Omega_0)$ or by replacing the transformation $T_{\mathcal{V}}$ with the composition $T_{\mathcal{V}} \circ T_{\mathcal{V}^*}$ (exploiting the fact that the composition of diffeomorphisms is again a diffeomorphism). This latter approach can be made computationally affordable by simply re-evaluating all $\mathbf{B}_i$'s on the mapped quadrature nodes; see the next paragraph on the computational complexity of Algorithm 1. Note also that Theorems 1 and 2 still hold as long as a finite number of compositions is considered.*

Finally, in line 8 we guarantee the admissibility of the optimization step δ according to the Armijo rule [20, Sect. 2.2.1.1].

In each iteration, the computational cost of the algorithm is mainly due to computing the finite element solution u_h in Line 5. Particularly costly are the assembly of the stiffness matrix and solving the linear system. The computational complexity of the latter depends only on the dimension of the finite elements trial space and can be reduced relying on iterative solvers or multigrid strategies; cf. [6]. On the other hand, the assembly of the stiffness matrix comprises numerical integration in each triangle and, thus, requires several calls of the costly matrix function $\mathbf{M}_{\mathcal{V}}$, whose entries are given as a sum of basis functions, and that has to be evaluated in each quadrature point. A first reduction of this computational cost can be achieved by realizing that, by the Hadamard-Zolésio structure theorem [14, Thm 2.4], only the B-splines whose supports intersect $\partial\Omega_0$ have to be taken into account. Nevertheless, we experienced that this is not enough to obtain reasonable computational times. Therefore, before starting the optimization routine, in Line 3 we pre-evaluate all B-splines in every quadrature point once and store the values.

[2]In practice, this condition can be tested only on a finite number of points. In our implementation we evaluate $\det \mathbf{D}T_{\mathcal{V}}$ on the FE quadrature points.

Algorithm 1 Gradient method with Armijo rule

1: Select initial design Ω_0, optimization step δ, and parameters ε,$\gamma \in (0,1)$
2: Initialize $\mathcal{V}_N = 0$, $\mathcal{V}_N^{\text{temp}} = 0$,
3: Precompute all $\mathbf{B}_i$'s on quadrature nodes
4: **for** $ii = 1, \ldots, MAX^{\text{ITER}}$ **do**
5: Compute finite element solution u_h of $\tilde{\mathcal{A}}_{\mathcal{V}} u = \tilde{f}_{\mathcal{V}}$ in Ω_0
6: Compute $\tilde{\mathcal{J}}^{\text{new}} = \tilde{\mathcal{J}}(\mathcal{V}_N^{\text{temp}}, u_h)$
7: **if** $ii > 1$ **and** $\tilde{\mathcal{J}}^{\text{new}} - \tilde{\mathcal{J}}^{\text{old}} > \gamma\delta d\tilde{J}(\mathcal{V}_N, u_h; \mathcal{V}_N^{\text{new}})$ **then**
8: Update $\delta = \delta/2$
9: **else**
10: Update $\delta = 2\delta$
11: Update $\mathcal{V}_N = \mathcal{V}_N^{\text{temp}}$, $\tilde{\mathcal{J}}^{\text{old}} = \tilde{\mathcal{J}}^{\text{new}}$
12: Compute $\mathcal{V}_N^{\text{new}} = \text{argmin}_{\mathcal{W}_N \in V_N, \|\mathcal{W}_N\|_{H^1(D)}=1} d\tilde{\mathcal{J}}(\mathcal{V}_N, u_h; \mathcal{W}_N)$
13: **end if**
14: Set $\mathcal{V}_N^{\text{temp}} = \mathcal{V}_N + \delta\mathcal{V}_N^{\text{new}}$
15: **while** $\min(\det \mathbf{D}T_{\mathcal{V}_N^{\text{temp}}}) < \varepsilon$ **do**
16: Update $\delta = \delta/2$ and set $\mathcal{V}_N^{\text{temp}} = \mathcal{V}_N + \delta\mathcal{V}_N^{\text{new}}$
17: **end while**
18: **end for**

Then, in each iteration, these values can be used to drastically reduce the computational cost of the matrix assembly, because the values of $\mathbf{M}_{\mathcal{V}}$ can be computed as linear combinations of the stored data. Additionally, these data can also be used to speed up both the computation of the descent direction in Line 12, which requires the evaluation of $d\tilde{\mathcal{J}}(\mathcal{V}, u_h; \mathbf{B}_i \mathbf{e}_j)$ for $i = 1, \ldots, N$, $j = 1, \ldots, d$, the feasibility test in Line 15, and the evaluation of the misfit functional $\tilde{\mathcal{J}}$ in Line 6. Note also that the memory requirement of this strategy can be reduced by exploiting the compact support property of B-splines: in each cell, just the B-splines whose support intersects that cell have to be evaluated on the quadrature points.

5 Numerical experiments

Let Ω_0 be an annular domain with internal boundary $\partial\Omega^{\text{in}}$ and external boundary $\partial\Omega^{\text{out}}$. The set of admissible domains is redefined to comprise domains obtained by perturbing only the external boundary $\partial\Omega^{\text{out}}$, i.e.,

$$\mathcal{U}_{\text{ad}}(\Omega_0) \coloneqq \{T_{\mathcal{V}}(\Omega_0); T_{\mathcal{V}} = \mathcal{I} + \mathcal{V}, \min(det\mathbf{D}T_{\mathcal{V}}) \geq \varepsilon, \operatorname{supp} \mathcal{V} \cap \partial\Omega^{\text{in}} = \emptyset\}\,. \tag{14}$$

We consider the shape optimization problem

$$\inf_{\Omega\in\mathcal{U}_{\rm ad}(\Omega_0)}\int_\Omega (\nabla u)^2 + g^2 \mathrm{d}\boldsymbol{x} \quad \text{subject to} \begin{cases} -\Delta u &= 0 \quad \text{in } \Omega\,, \\ u &= 0 \quad \text{on } \partial\Omega^{\rm out}\,, \\ u &= 1 \quad \text{on } \partial\Omega^{\rm in}\,, \end{cases} \tag{15}$$

where g is a constant.

Such an optimization problem stems from the class of Bernoulli exterior free boundary problems, which are used as a benchmark in shape optimization because they admit stable minimizers. This is due to the $H^{1/2}(\partial\Omega_0)$-coercivity (see Equation (12)) of its Hessian in the optimal shape [16].

The parametric form of (15) reads

$$\inf_{\Omega\in\mathcal{U}_{\rm ad}(\Omega_0)}\int_{\Omega_0} \nabla u\cdot \boldsymbol{M}_{\mathcal{V}}\nabla u + g^2 |\det \mathbf{D}T_{\mathcal{V}}| \mathrm{d}\boldsymbol{x} \tag{16}$$
$$\text{subject to} \quad \begin{cases} -\operatorname{div}\mathbf{M}_{\mathcal{V}}\,\mathbf{grad}\, u &= 0 \quad \text{in } \Omega_0\,, \\ u &= 0 \quad \text{on } \partial\Omega_0^{\rm out}\,, \\ u &= 1 \quad \text{on } \partial\Omega_0^{\rm in}\,, \end{cases}$$

where $\mathbf{M}_{\mathcal{V}} \coloneqq (\det \mathbf{D}T_{\mathcal{V}})\mathbf{D}T_{\mathcal{V}}^{-1}\mathbf{D}T_{\mathcal{V}}^{-T}$. The Fréchet derivative of the shape functional in (16) reads

$$d\tilde{\mathcal{J}}(\mathcal{V},u;\mathcal{W}) = \int_{\Omega_0} \nabla u\cdot(\partial_{\mathcal{W}}\mathbf{M}_{\mathcal{V}})\nabla u + g^2(\partial_{\mathcal{W}}\det\mathbf{D}T_{\mathcal{V}})\,\mathrm{d}\boldsymbol{x}\,. \tag{17}$$

Note that, in contrast to Example 2, formula (17) does not involve the solution of an adjoint problem [17].

Henceforth, we set $g = (1.2\ln(2.4))^{-1}$, so that the external boundary of the optimal solution is a circle of radius 1.2 centered in the origin. In all the experiments, we consider finite element solutions computed with linear Lagrangian finite elements on quasi-uniform triangular meshes. Integrals in the domain are computed by a 3-point quadrature rule of order 3 in each triangle. The boundary of the computational domain is approximated by a polygon, which will not affect the convergence of linear finite elements [10, Sect. 10.2]. The optimization step δ is initially set to $\delta = 0.3$ and the parameter ε to $\varepsilon = 0.1$. Finally, instead of the Armijo rule condition, we just check that the absolute error does not increase in line 8 of Algorithm 1 on page 11.

To show that the algorithm proposed in Section 4 is feasible, we select $\partial\Omega_0^{\rm out}$ to be an ellipse with major semi-axis of length 1.5 and minor semi-axis of length 1.3, whilst $\partial\Omega_0^{\rm out}$ is a circle of radius 0.5 centered in the origin (see Figure 1). The domain Ω_0 is covered with a regular grid of width 0.255 over

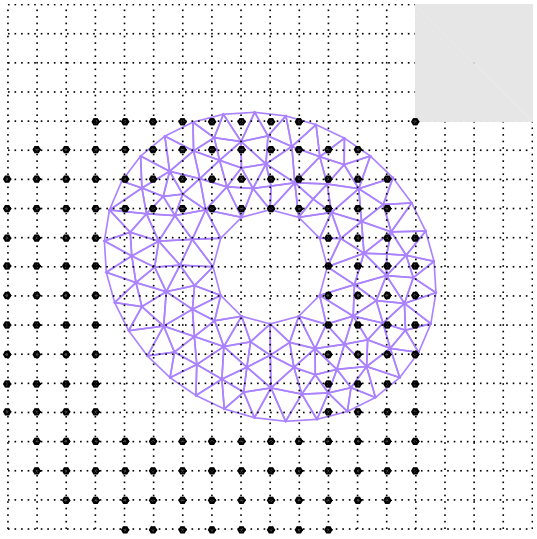

Figure 1: The initial guess Ω_0 is covered with a regular grid used to generate cubic B-splines. Dots indicate the lower left corner of the support of the active B-splines. The square in the top right corner indicates the support of a cubic B-spline. A triangular grid is generated on Ω_0 to compute the finite element solution u_h.

which the trial space V_N is constructed. The finite element solution u_h is computed on the mesh displayed in Figure 1. Despite the coarseness of the mesh and the low resolution of the B-spline grid, after twelve optimization steps we already recover a satisfactory approximation of the target boundary; see Figure 2 (left).

The experiment is repeated for a different initial design (a square with edges of length 2.06). Again, after twelve steps we recover a satisfactory approximation of the target boundary; see Figure 2 (right).

Next, we investigate the impact of the finite element approximation on the retrieved approximate optimal solution. We keep the trial space of B-splines V_N fixed (with width 0.255), and we generate 7 additional meshes through uniform refinement of the one displayed in Figure 1 (during the refinement the boundary nodes are projected onto $\partial\Omega_0$). Let

$$\mathrm{err}^{(i)} := \frac{\left|\tilde{\mathcal{J}}(\mathcal{V}_N^{(i)}, u_h) - \tilde{\mathcal{J}}_{\min}\right|}{\tilde{\mathcal{J}}(\mathcal{I}, u_h)} \tag{18}$$

be the scaled absolute error obtained after i steps of Algorithm 1. In Figure 3 (left) we plot the the evolution of $\mathrm{err}^{(i)}$ for each mesh. In Figure 3 (right) we plot $\mathrm{err}^{(60)}$ for each mesh versus its mesh width. We observe an alge-

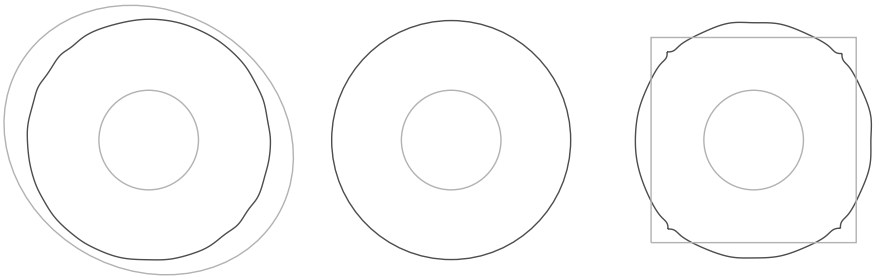

Figure 2: Approximate optimal boundary retrieved after twelve iterations of Algorithm 1 for numerical experiment 1 (*left*) and 2 (*right*). Despite the coarseness of the mesh and the low resolution of the B-spline grid, we recover a decent approximation (dark gray line) of the optimum (exterior boundary of the annulus in the middle). Light gray lines indicate the boundary of the initial guess Ω_0.

braic convergence with rate 1.7. We remark that $\tilde{\mathcal{J}}(\mathcal{V}, u_h)$ itself converges quadratically in the mesh width h (uniformly in $\mathcal{V} \in C^2(\overline{D}; \mathbb{R}^d)$).

Then, we investigate the impact of the resolution provided by V_N on the approximate optimal solution. We perform the experiment on the fourth mesh of the previous experiment. In Figure 4 we show the evolution of $\mathrm{err}^{(i)}$ for V_N constructed on a regular grid of width 0.51 (–▲–) and 0.255 (–■–). The former trial space comprises 54 active basis function, whilst the latter has 152 active basis functions. We see that the resolution of V_N affects the quality of the retrieved approximate optimal solution. However, it is not easy to guess the optimal resolution of V_N. A fine regular grid produces basis functions with small support, and thus, with higher $C^1(\overline{D}; \mathbb{R}^d)$-norm (for fixed $C^0(\overline{D}; \mathbb{R}^d)$-norm). This is reflected in smaller values of $\det T_{\mathcal{V}}$, because we drop all B-splines whose support does not intersect $\partial\Omega_0$ since they lie in the kernel of $d\tilde{\mathcal{J}}$. There is, hence, a trade-off between the resolution of the spline space and the maximal displacement that it can reproduce. Therefore, we suggest to pursue an adaptive strategy by starting with a relatively coarse resolution and, when the iteration stagnates, to embed the so far computed discrete vector field on a nested space spanned by basis functions generated on a grid with half the meshwidth [22, Sect. 7.6]. Then, new descent directions are computed by taking into account only the new basis functions that intersect the boundary, whilst the ones that do not intersect the boundary

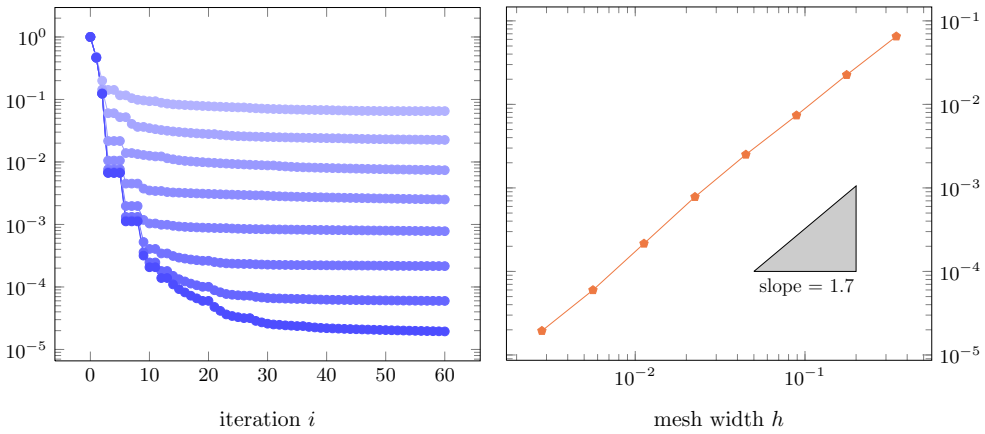

Figure 3: *Left:* Evolution of the scaled absolute error (18) on 8 nested meshes obtained with uniform refinement. *Right:* Value of scaled absolute error versus meshwidth at 60th iteration. We observe algebraic convergence with rate 1.7 (superconvergence).

are kept to provide a smoother decay of the vector field. The evolution of $\mathrm{err}^{(i)}$ for this strategy is displayed in Figure 4 (—●—). We see that we are able to improve the quality of the approximate optimal solution by switching to a finer space after 10 iterations.

Finally, we test our algorithm on a prototypical ill-posed inverse problem. Let B be a fixed subdomain of a domain Ω and let $u_t \in L^2(B)$ be a given target function. The goal is to find the optimal domain that contains B, so that the shape functional

$$\mathcal{J}(\Omega) := \int_B (u - u_t)^2 \mathrm{d}\boldsymbol{x}\,, \quad \text{subject to} \quad -\Delta u = 1 \text{ in } H_0^1(\Omega)\,, \tag{19}$$

attains its minimum.

As explained in [12], elliptic regularity theory implies that the solution u of the state problem is in $H^2(\Omega)$ as soon as Ω is of class C^2. Therefore, the range of the operator $\mathcal{V} \mapsto u|_B$ is at most a dense subset of $L^2(\Omega)$ [9, Thm. 7.2]. Thus, the shape optimization problem (19) is ill-posed. An alternative exposition of the ill-posedness of (19) from a shape optimization point of view can be found in [15].

Similar to Example 2, the shape derivative of the shape optimization problem (19) recast in parametric form reads

$$d\tilde{\mathcal{J}}(\mathcal{V}, u; \mathcal{W}) = \int_{\Omega_0} \mathbf{grad}\, p \cdot \partial_{\mathcal{W}} \mathbf{M}_{\mathcal{V}}\, \mathbf{grad}\, u - p\, \partial_{\mathcal{W}}(\det \mathbf{D}T_{\mathcal{V}})\, \mathrm{d}\boldsymbol{x}\,,$$

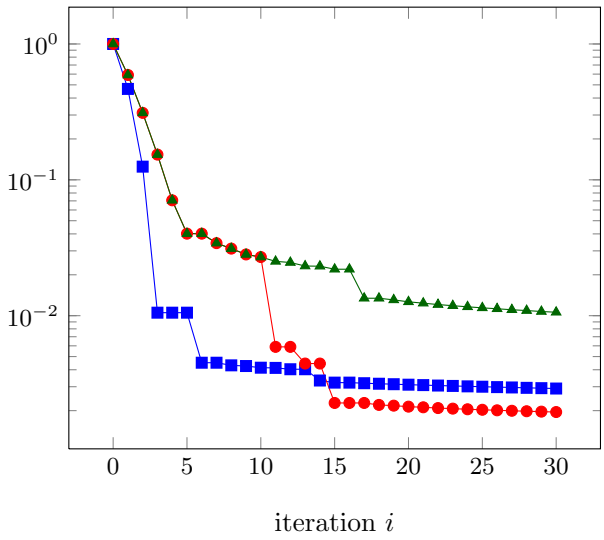

Figure 4: Evolution of the scaled absolute error (18) for a coarse (–▲–) and a finer (–■–) trial space V_N. Switching to a finer space after 10 iterations, it is possible start with a coarse trial space and still retrieve an approximate solution with good quality (–●–).

where u and p are the solutions of

$$\begin{aligned} -\operatorname{div}(\mathbf{M}_{\mathcal{V}} \operatorname{\mathbf{grad}} u) &= \det \mathbf{D}T_{\mathcal{V}} && \text{in } H_0^1(\Omega)\,, \\ -\operatorname{div}(\mathbf{M}_{\mathcal{V}} \operatorname{\mathbf{grad}} p) &= -\chi_B 2(u - u_t) && \text{in } H_0^1(\Omega)\,. \end{aligned}$$

Note that here the set of admissible shapes reads

$$\mathcal{U}_{\text{ad}}(\Omega_0) \coloneqq \{T_{\mathcal{V}}(\Omega_0); T_{\mathcal{V}} = \mathcal{I} + \mathcal{V}, \min(\det \mathbf{D}T_{\mathcal{V}}) \geq \varepsilon, \operatorname{supp} \mathcal{V} \cap B = \emptyset\}\,.$$

In particular, we consider only vector fields that vanish on B because the latter denotes the region of interest and is assumed to be fixed.

The goal of this experiment is to asses the relevance of the regularization provided by the choice of $H_0^1(\overline{D}; \mathbb{R}^d)$-representatives of the Fréchet derivative; see Equation (13). We set $u_t(\mathbf{x}) \coloneqq (1.2)^2/4 - \mathbf{x} \cdot \mathbf{x}/4$, so that an optimal domain is the disc centered in 0 with radius 1.2. The region of interest B is a disc centered in 0 with radius 0.5 whilst the initial domain Ω_0 is a disc centered in 0 with radius 1.3. We decide to start with Ω_0 close to the optimum because we construct the B-splines on a very fine grid in order to exclude discretization by regularization. To be precise, we set the gridwidth to 0.051, which corresponds to 729 active B-splines, and thus to 1458 basis

vector fields; see Equation (10). The finite element mesh has 8001 nodes and 15744 triangles.

In Figure 5 we display the evolution of: the shape functional J (–▲–), the minimal value of $\det \mathbf{D}T_{\mathcal{V}}$ on the quadrature points (–■–), the optimization step δ (–●–). The graph on the left refers to the $H_0^1(\overline{D};\mathbb{R}^d)$-representative whilst the one on the right to the "Euclidean"-representative[3]. For a better comparison, the $H_0^1(\overline{D};\mathbb{R}^d)$-representatives have been additionally normalized with respect to the Euclidean norm. When the $H_0^1(\overline{D};\mathbb{R}^d)$-metric is employed, we clearly see that the algorithm succeeds in reconstructing the target shape (small values of J) and that the descent directions give rise to feasible transformations ($\min(\det \mathbf{D}T_{\mathcal{V}})$ is bigger than the threshold $\varepsilon = 0.05$) without making the optimization step δ decay rapidly to 0. From the third iteration on, updates on δ occur just to fulfill the Armijo rule, as can be see from the stagnation of the values of J. On the other hand, the optimization step δ has to decrease rapidly to make the transformations $T_{\mathcal{V}}$ feasible when the algorithm relies on Euclidean-representatives of the Fréchet derivative. This drastically slows down the reconstruction of the optimal shape, and corroborates the regularizing properties provided by the use of the $H_0^1(\overline{D};\mathbb{R}^d)$-metric.

6 Conclusions

We presented a method to compute approximate optimal solutions of elliptic PDE constrained shape optimization problems. Shapes are identified with diffeomorphisms and the shape optimization problem is recast as an optimal control problem. The latter is then stated on a finite dimensional trial space based on cubic B-splines pursuing a Ritz approach. Under reasonable assumptions, the solution of the finite dimensional problem converges to the solution of the original problem.

To solve the finite dimensional problem we rely on descent methods. We employ $H_0^1(\overline{D};\mathbb{R}^d)$-representatives of the Fréchet derivative. For well-posed shape optimization problems, this choice is consistent with the coercivity estimate (12) fulfilled by the shape Hessian. For ill-posed problems, it provides a regularization in the spirit of regularized sequential quadratic programming.

Superconvergence in the approximation of the Fréchet derivative can be achieved relying on FE discretizations of the underlying BVP. Numerical experiments show that accuracy in the approximation of the Fréchet derivative directly affects the quality of the retrieved approximate optimal solution.

[3]By "Euclidean"-representative we mean that the coefficients in the representation (10) of the descent direction are set to $c_i^j = d\tilde{\mathcal{J}}(\mathcal{V};\mathbf{B}_i\mathbf{e}_j)$.

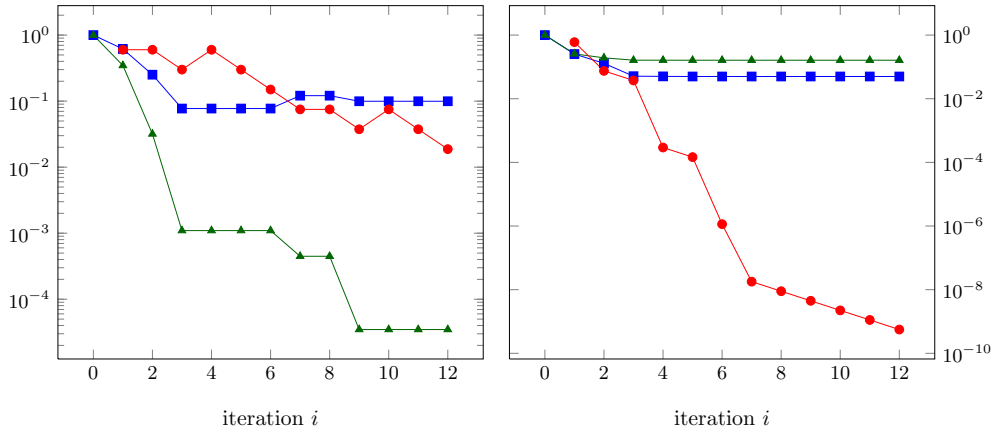

Figure 5: Evolution for the ill-posed shape optimization problem (19) of: the shape functional J (▲), the minimal value of $\det(\mathbf{D}T_{\mathcal{V}})$ on the quadrature points (■), and of the optimization step δ (●) for descent directions computed with respect to the $H_0^1(\overline{D};\mathbb{R}^d)$ (*left*) and the Euclidean metric (*right*). Due to the ill-posed nature of the shape optimization problem, the optimization step δ has to decrease rapidly to make the transformations $T_{\mathcal{V}}$ feasible in absence of regularization.

Finally, we discussed an adaptive strategy based on nested trial spaces to balance discretization errors due to B-splines approximation of shapes and FE approximations of the solution of the PDE constraint.

Acknowledgments

The authors thank Andreas Hiltebrand for fruitful discussions on implementation aspects. Alberto Paganini acknowledges RICAM fellowship for the Special Semester on Calculus of Variations, during which part of this work was completed.

References

[1] R. A. Adams and J. J. F. Fournier, *Sobolev spaces*, vol. 140 of Pure and Applied Mathematics (Amsterdam), Elsevier/Academic Press, Amsterdam, second ed., 2003.

[2] G. Allaire, *Conception optimale de structures*, vol. 58 of Mathématiques & Applications (Berlin) [Mathematics & Applications],

Springer-Verlag, Berlin, 2007. With the collaboration of Marc Schoenauer (INRIA) in the writing of Chapter 8.

[3] G. Allaire, C. Dapogny, and P. Frey, *Topology and geometry optimization of elastic structures by exact deformation of simplicial mesh*, Comptes Rendus Mathematique, 349 (2011), pp. 999 – 1003.

[4] G. Allaire, C. Dapogny, and P. Frey, *Shape optimization with a level set based mesh evolution method*, Computer Methods in Applied Mechanics and Engineering, 282 (2014), pp. 22 – 53.

[5] G. Allaire, F. Jouve, and A.-M. Toader, *Structural optimization using sensitivity analysis and a level-set method*, J. Comput. Phys., 194 (2004), pp. 363–393.

[6] P. F. Antonietti, A. Borzì, and M. Verani, *Multigrid shape optimization governed by elliptic PDEs*, SIAM J. Control Optim., 51 (2013), pp. 1417–1440.

[7] F. Ballarin, A. Manzoni, G. Rozza, and S. Salsa, *Shape optimization by free-form deformation: existence results and numerical solution for Stokes flows*, J. Sci. Comput., 60 (2014).

[8] D. Begis and R. Glowinski, *Application de la méthode des éléments finis à l'approximation d'un problème de domaine optimal. Méthodes de résolution des problèmes approchés*, Applied Mathematics and Optimization, 2 (1975), pp. 130–169.

[9] D. Braess, *Finite elements. Theory, fast solvers, and applications in elasticity theory*, Cambridge University Press, third ed., 2007.

[10] S. C. Brenner and L. R. Scott, *The mathematical theory of finite element methods*, vol. 15 of Texts in Applied Mathematics, Springer, New York, third ed., 2008.

[11] M. Burger and W. Mühlhuber, *Iterative regularization of parameter identification problems by sequential quadratic programming methods*, Inverse Problems, 18 (2002), pp. 943–969.

[12] D. Chenais and E. Zuazua, *Controllability of an elliptic equation and its finite difference approximation by the shape of the domain*, Numer. Math., 95 (2003), pp. 63–99.

[13] M. Dambrine and M. Pierre, *About stability of equilibrium shapes*, M2AN Math. Model. Numer. Anal., 34 (2000), pp. 811–834.

[14] M. C. Delfour and J.-P. Zolésio, *Velocity method and Lagrangian formulation for the computation of the shape Hessian*, SIAM J. Control Optim., 29 (1991), pp. 1414–1442.

[15] K. Eppler and H. Harbrecht, *Coupling of FEM and BEM in shape optimization*, Numer. Math., 104 (2006), pp. 47–68.

[16] ——, *Shape optimization for free boundary problems—analysis and numerics*, in Constrained optimization and optimal control for partial differential equations, vol. 160 of Internat. Ser. Numer. Math., Birkhäuser/Springer Basel AG, Basel, 2012, pp. 277–288.

[17] K. Eppler, H. Harbrecht, and R. Schneider, *On convergence in elliptic shape optimization*, SIAM J. Control Optim., 46 (2007), pp. 61–83 (electronic).

[18] I. Fumagalli, N. Parolini, and M. Verani, *Shape optimization for stokes flow: a reference domain approach.* arXiv:1403.3540 [math.NA], 2014.

[19] I. M. Gelfand and S. V. Fomin, *Calculus of variations*, Revised English edition translated and edited by Richard A. Silverman, Prentice-Hall, Inc., Englewood Cliffs, N.J., 1963.

[20] M. Hinze, R. Pinnau, M. Ulbrich, and S. Ulbrich, *Optimization with PDE constraints*, vol. 23 of Mathematical Modelling: Theory and Applications, Springer, New York, 2009.

[21] R. Hiptmair, A. Paganini, and S. Sargheini, *Comparison of approximate shape gradients*, BIT Numerical Mathematics, (2014), pp. 1–27.

[22] K. Höllig and J. Hörner, *Approximation and modeling with B-splines*, Society for Industrial and Applied Mathematics, Philadelphia, PA, 2013.

[23] B. Kiniger and B. Vexler, *A priori error estimates for finite element discretizations of a shape optimization problem*, ESAIM Math. Model. Numer. Anal., 47 (2013), pp. 1733–1763.

[24] T. Lassila and G. Rozza, *Parametric free-form shape design with PDE models and reduced basis method*, Comput. Methods Appl. Mech. Engrg., 199 (2010), pp. 1583–1592.

[25] P. Morice, *Une methode d'optimisation de forme de domaine*, in Control Theory, Numerical Methods and Computer Systems Modelling, Springer Berlin Heidelberg, 1975.

[26] O. Pironneau, *Optimal shape design for elliptic systems*, in System Modeling and Optimization, Springer Berlin Heidelberg, 1982.

[27] J. A. Sethian, *Level set methods and fast marching methods*, Cambridge University Press, Cambridge, 1999.

[28] M. Souli and J.-P. Zolésio, *Shape derivative of discretized problems*, Comput. Methods Appl. Mech. Engrg., 108 (1993), pp. 187–199.

Recent Research Reports

Nr.	Authors/Title

2014-17 A. Hiltebrand and S. Mishra
Efficient computation of all speed flows using an entropy stable shock-capturing space-time discontinuous Galerkin method

2014-18 D. Conus and A. Jentzen and R. Kurniawan
Weak convergence rates of spectral Galerkin approximations for SPDEs with nonlinear diffusion coefficients

2014-19 J. Doelz and H. Harbrecht and Ch. Schwab
Covariance regularity and H-matrix approximation for rough random fields

2014-20 P. Grohs and S. Hosseini
Nonsmooth Trust Region Algorithms for Locally Lipschitz Functions on Riemannian Manifolds

2014-21 P. Grohs and A. Obermeier
Optimal Adaptive Ridgelet Schemes for Linear Transport Equations

2014-22 S. Mishra and Ch. Schwab and J. Sukys
Multi-Level Monte Carlo Finite Volume methods for uncertainty quantification of acoustic wave propagation in random heterogeneous layered medium

2014-23 J. Dick and Q. T. Le Gia and Ch. Schwab
Higher order Quasi Monte Carlo integration for holomorphic, parametric operator equations

2014-24 C. Sanchez-Linares and M. de la Asunci on and M. Castro and S. Mishra and J. Šukys
Multi-level Monte Carlo finite volume method for shallow water equations with uncertain parameters applied to landslides-generated tsunamis

2014-25 R.N. Gantner and Ch. Schwab
Computational Higher Order Quasi-Monte Carlo Integration

2014-26 C. Schillings and Ch. Schwab
Scaling Limits in Computational Bayesian Inversion